Copper Oxide Nanomaterial Fate in Plant Tissue: Nanoscale Impacts on Reproductive Tissues

Copper Oxide nanomaterial fate in plant tissue: Nanoscale impacts on reproductive tissues

Journal:	*Environmental Science & Technology*
Manuscript ID	es-2021-01123t.R1
Manuscript Type:	Article
Date Submitted by the Author:	13-May-2021
Complete List of Authors:	Marmiroli, Marta; Universita degli Studi di Parma, Dept. Environmental Sciences Pagano, Luca; University of Parma, Chemistry, Life Science and Environmental Sustainability Rossi, Riccardo; University of Parma De la Torre-Roche, Roberto; Connecticut Agricultural Experiment Station Lepore, Giovanni Orazio; Università degli Studi di Firenze, Dipartimento di Scienze della Terra Ruotolo, Roberta ; Universita degli Studi di Parma, of Chemistry, Life Sciences and Environmental Sustainability Gariani, Gianluca; Elettra Sincrotrone Trieste SCpA Bonanni, Valentina; Elettra Sincrotrone Trieste SCpA Pollastri, Simone; Elettra Sincrotrone Trieste SCpA, Puri, Alessandro; ESRF Gianoncelli, Alessandra; Elettra - Sincrotrone Trieste S.C.p.A., ELETTRA, Aquilanti, Giuliana; Elettra-Sincrotrone Trieste, D'Acapito, Francesco; ESRF, White, Jason; Connecticut Agricultural Experiment Station, Department of Analytical Chemistry Marmiroli, Nelson; Universita degli Studi di Parma, Department of Chemistry, Life Sciences and Environmental Sustainability

Copper Oxide nanomaterial fate in plant tissue: Nanoscale impacts on reproductive tissues

Marta Marmiroli,[1,*] Luca Pagano,[1,*] Riccardo Rossi,[1] Roberto De La Torre-Roche,[2] Giovanni Orazio Lepore,[3] Roberta Ruotolo,[1] Gianluca Gariani,[4] Valentina Bonanni,[4] Simone Pollastri,[4] Alessandro Puri,[5] Alessandra Gianoncelli,[4] Giuliana Aquilanti,[4] Francesco d'Acapito,[5] Jason C. White,[2,§] Nelson Marmiroli[1,6,§,#]

[1] Department of Chemistry, Life Sciences and Environmental Sustainability, University of Parma, Parco Area delle Scienze 11/A, 43124 Parma, Italy.

[2] The Connecticut Agricultural Experiment Station, 123 Huntington Street, 06504 New Haven, CT, USA.

[3] Earth Science Department, Univeristy of Florence, Via La Pira 4, 50121 Firenze, Italy.

[4] Elettra, Sincrotrone Trieste, Strada Statale 14 - km 163,5 in AREA Science Park, 34149 Trieste, Italy.

[5] CNR-IOM-OGG c/o ESRF – The European Synchrotron, 71 Avenue des Martyrs CS 40220, F-38043 Grenoble Cédex 9, France.

[6] Consorzio Interuniversitario Nazionale per le Scienze Ambientali (CINSA), University of Parma, 43124 Parma, Italy.

* co-first authorship.

§ co-last authorship.

corresponding author, nelson.marmiroli@unipr.it.

Abstract

A thorough understanding of the implications of chronic low dose exposure to Engineered Nanomaterials (ENMs) through the food chain is lacking. The present study aimed to characterize such response in *Cucurbita pepo* L. (zucchini) upon exposure to a potential nanoscale fertilizer: copper oxide (CuO) nanoparticles. Zucchini was grown in soil amended with nano-CuO, bulk CuO (100 mg Kg^{-1}) and $CuSO_4$ (320 mg Kg^{-1}) from germination to flowering (60 days). Nano-CuO treatment had no impact on plant morphology or growth, nor pollen formation and viability. The uptake of Cu was comparable in the plant tissues under all treatments. RNA-seq analyses on

vegetative and reproductive tissues highlighted common and nanoscale-specific component of the response. Mitochondrial and chloroplast functions were uniquely modulated in response to nanomaterial exposure as compared with conventional bulk and salt forms. X-ray Absorption Spectroscopy (XAS) showed that Cu local structure changed upon nano-CuO internalization, suggesting potential nanoparticles biotransformation within the plant tissues. These findings demonstrate the physiological, cellular, and molecular consequences related to nano-CuO application as a plant fertilizer, highlighting the differential mechanisms involved in the exposure to nano-CuO, bulk or salt and the pathways of plant response to minimize environmental and health risk, through sustainable nano-enabled agricultural strategies.

Keywords: nanomaterials, nanofertilization, RNA-seq, pollen, biotransformation, *Cucurbita pepo.*

Synopsis

Fertilization with nanoscale CuO affected zucchini at the physiological and molecular levels, from roots to flowers, with significant internalization and particle biotransformation being evident.

Introduction

In recent years, interest in the utilization of nanotechnology to produce nano-enabled materials and delivery platforms to address the progressive inefficiency of mineral fertilization has been rapidly growing.[1,2] However, these nanomaterials are by their very nature more reactive and bioavailable than traditional forms utilized in agriculture,[1-3] and as such, have raised concerns over sustainability and safety with regard to human and environmental health. For example, direct utilization in agriculture raises the clear possibility of food chain contamination from staple plants to humans through the direct consumption of contaminated plant products as could happen with rice, maize and peanuts.[3,4] In addition, the potential widespread use of engineered nanomaterials (ENMs) as part of "nano-agricultural chemistry" has created concerns over damage to non-target organisms and to potential trophic transfer through terrestrial food chains, through vegetables grazing by simple insects and then spreading out to higher insects and predators.[5-9] As such, safety assessment and sustainability evaluation must be a core component in novel materials formulations for agri-food production purposes (e.g. nanopesticides, nanofertilizers). [1,10-13]

A number of recent studies have demonstrated the unique potential of Cu-based nanomaterials in agriculture,[11,14,15] including field studies demonstrating how materials such as $Cu_3(PO4)_2$ based-nanosheets and commercial CuO NPs can be foliar applied to young seedlings so as to increase plant growth and suppress *Fusarium* spp. infections of tomato (*Solanum lycopersicum* L.) and watermelon (*Citrullus lanatus* L.) in full life cycle studies. Furthermore, Ma *et al*. (2020)[13] studied how nanomaterial chemistry could be tuned to optimize the effects of pathogen suppression and nutrient release from Cu-based ENMs on sudden death syndrome (SDS) in soybean (*Glycine max* L.), developing a thermodynamic model to describe how morphology and matrix effects are implicated in Cu release and plant response. In addition, Cu-based nanoformulations are known to interact with organic acids in plant root exudates. These interactions significantly influence ENM stability, biotransformation and bioavailability,[16] as well as induce modifications in the plant metabolome.[17]

The role of Cu nanomaterial bioavailability has also been investigated through trophic transfer experiments, including an assessment of how initial chemical form is impacted by relevant weathering conditions and subsequent material transformation.[18] These findings highlight the importance of controlling ENMs physico-chemical properties (e.g. morphology, composition and dissolution) so as to develop safer and more sustainable nanoscale formulations for agriculture, simultaneously enhancing the targeting and delivery efficiency to optimize utilization of resources while minimizing negative impacts on the environment.[1]

The current study investigated the potential effects of CuO NPs on zucchini (*Cucurbita pepo* L.) from a morphological, physiological, molecular, and atomic perspective, with a particular focus on gametogenesis and pollen development. Conventional CuO bulk material and $CuSO_4$ salts were used as controls to clarify nanoscale-specific effects of CuO NPs with regard to its fate within the plant tissues. Particular attention was focused on the function and regulation of chloroplast and mitochondrion activity, which play a critical role in pollen development. The coupling of a global transcriptomic approach (by RNA-seq) with synchrotron-based analyses, such as μ-X-ray Fluorescence (μ-XRF) mapping and Extended X-ray absorption fine structure (EXAFS) spectroscopy of Cu states, enabled a thorough understanding of the connection between the observed biological response and the physico-chemical condition of CuO NPs at a molecular and sub-molecular level in different plant tissues.

Methods

Nanomaterial characterization

Copper oxide nanoparticles (CuO NPs) (99% purity; 40 nm average sized) were purchased from U.S. Research Nanomaterials, Inc. (Houston, TX). Cu represents 79.8% of the total molecular weight of the molecule. CuO NPs were characterized by electron microscopy (TEM, Talos F200S G2, SEM FEG Thermo Fisher Scientific, Waltham, MA, USA) as reported in Figure S1. The average particle size (*dh*) and zeta (ζ) potential in ddH_2O were 533.9 ± 47.2 nm and of -24.7 ± 1.4 mV as

106 determined by Zetasizer Nano Series ZS90 (Malvern Instruments, Malvern, UK), after sonication by
107 a Fisher Scientific Model 505 Sonic Dismembrator (Fisher Scientific, Waltham, MA) at 40%
108 amplitude for 60s. CuO bulk material and $CuSO_4 \cdot 5H_2O$ were purchased from Sigma Aldrich (St.
109 Louis, MO, US).

110 For particle dissolution analysis, CuO NPs and CuO bulk solutions (1000 mg L^{-1}) were
111 prepared in ddH_2O, avoiding shaking and light, and portions were collected after 1, 2, 3, 7, and 14d.
112 Aliquots of 1 ml for each sample were precipitated by ultracentrifugation at 30000 rpm, for 10 min,
113 at 20°C (Optima Max-XP Ultracentrifuge, Beckman-Coulter Inc., Brea, CA, USA). The liquid phase
114 was collected and digested in 4 mL of 1M HNO_3 (purity: 67% w/w) for 40 min at 200°C using a
115 VELP DK20 digester (VELP Scientifica, Usmate, Italy). The digests were analysed by flame atomic
116 absorption spectroscopy (FA-AAS; AA240FS, Agilent Technologies, Santa Clara, CA, USA) for the
117 presence of Cu (lamp current: 4 mA; fuel: acetylene; support: air; wavelength 324.7 nm; slit with: 0.5
118 nm; linearity of calibration, R^2: 0.9982), in three replicates. The average dissolution for CuO bulk
119 and CuO NPs were between 0.1% and 0.15%, respectively, considering the theoretical value of 100%
120 dissolution of ionic copper in $CuSO_4$.

121

122 *Plant exposure*

123 *Cucurbita pepo* L. (cv. Costata Romanesco) seeds were pre-germinated in vermiculite
124 amended with Hoagland's Solution (10%) for 10 days prior to transplanting to soil. The Cu
125 concentration administered in pre-germination was about 2 μg Kg^{-1}. Zucchini seeds were purchased
126 from Johnny's Selected Seeds (Albion, ME, USA). The experimental soil was collected from the
127 Connecticut Agricultural Experiment Station (CAES) Lockwood Farm in Hamden, CT, USA.
128 Individual solutions of CuO NPs and CuO bulk material in water (30% water capacity of
129 soil/vermiculite mixture) were probe sonicated by a Fisher Scientific Model 505 Sonic Dismembrator
130 (Fisher Scientific, Waltham, MA) at 40% amplitude for 60−120s to maximize dispersion. Solutions

of CuO NPs, CuO (bulk) or (copper sulfate) $CuSO_4$ were slowly added to pots containing 500g of soil and manually mixed. The final concentration of NPs and bulk CuO in pots was 100 mg kg^{-1} while for $CuSO_4 \cdot 5H_2O$ (copper sulfate pentahydrate), the amount was 320 mg kg^{-1}. Considering the molecular weight of the single molecules taken into account, this represented a total concentration of approximately 80 mg kg^{-1} for all the treatments. Additional data related to the Cu release in treated soils are reported in Supporting Information (SI). The concentrations utilized were chosen to be below the limit considered as potential Cu contamination in soil, and yet still able to provide information on chronic plant exposure.[19-20] Furthermore, the low dose utilized and the long growth period (60 days) are indicative of a chronic exposure scenario that is not common in the literature.[21] Zucchini seedlings were planted (one each pot) and grown indoor under supplemental fluorescent lighting (60 μE m^2 sec) under a photoperiod of 16h light at approximately 22−28 °C until flowering. Plants were top watered during a 60-d growth period. For all the conditions, ten biological replicates were included.

Pollen morphology and pollen viability

Alexander's staining protocol was used to test pollen viability. Free anthers were collected when pollen was mature but anthers were still non-dehiscent (stage 12-13), and were fixed in Carnoy's fixative (6 ethanol: 3 chloroform: 1 acetic acid) for 2h. Mature pollen was collected and stained as described in Peterson *et al.* (2010).[22] After staining, all aborted and non-aborted pollen grains were counted using a Zeiss Apotome 2 microscope at 20x magnification (Zeiss, Oberkochen, Germany). Pollen grains were analysed fresh with no fixation or staining; they were collected from mature flowers and positioned on 2 cm diameter stainless-steel sample holder (stub) covered with adhesive carbon tape. An environmental scanning electron microscope (ESEM) FEG2500 FEI (FEI Europe, Eindhoven, The Netherlands) operating in low-vacuum (60 Pa) with LFD (Large Field Detector) was used to enable optimal Secondary Electron (SE) imaging. The cone PLA (Pressure Limiting Aperture) of 500 μm improved the signal available to the Bruker X-ray detector,

QUANTAX XFlash. SE imaging was performed at 10 KeV with a beam size of 2.5 µm, EDX analysis at 20 KeV acceleration voltage, final lens aperture of 40 µm, and beam size of 4 µm. SE images and EDX spectra were collected from samples treated with CuO NPs, CuO bulk and untreated controls.

Metal uptake measurement

Flowers harvested for elemental analyses were sampled and thoroughly rinsed with tap water, MilliQ water (resistivity: 18.2 MΩ cm) and 2% HNO_3 (0.01 M) to remove soil and surface-attached NPs. To determine Cu content in the tissues, fresh samples were dried at 100 °C for 72 h and digested in HNO_3 (purity: 67% w/w) at 115 °C, 25 min. After 30 min, 1 mL of H_2O_2 (purity: 30 % w/w) was added to each digestion tube and the samples treated for an additional 30 min prior dilution to 50 mL with ddH_2O. The digested samples from the 10 biological replicates per treatment were analysed by inductively coupled plasma mass spectrometry (ICP-MS) Agilent 7500ce (Agilent Technologies, Santa Clara, CA) for Cu presence (63 amu). The digests Cu content were quantified against a five-point calibration curve based on certified reference material (SPEX CertiPrep, Metuchen, NJ, USA), and that had been previously evaluated for linearity (R^2: 0.9999) and accuracy. Analytical blanks, matrix blanks, and calibration verification samples were included in each sequence.

Roots, stems, leaves and flower biomass samples were collected after 60-d for elemental analysis. Samples (10 replicates for each tissue) were digested as in the case of ICP-MS analyses and analysed by Atomic Absorption Spectroscopy (AAS) (AA240FS device, Agilent Technologies, Santa Clara, CA; lamp current: 4 mA; fuel: acetylene; support: air; wavelength 324.7 nm; slit with: 0.5 nm; linearity of calibration, R^2: 0.9993). AAS analyses were conducted with a four-point calibration curve based on standard reference material (SPEX CertiPrep, Metuchen, NJ). Biomass and Cu content in all tissues were evaluated by a one-way ANOVA with a pairwise Tukey's multiple comparison test (IBM SPSS v. 26.0).

RNA extraction and whole transcriptome analysis

RNA samples were extracted from 0.1g (fresh weight) of pollen, leaves or roots samples from unamended control, CuO NP, CuO bulk and $CuSO_4$ treatments. Total RNA was extracted from 0.1 g of fresh plant material using a Sigma-Aldrich Spectrum Plant Total RNA Kit (Sigma-Aldrich, St. Louis, MO). Three biological replicates per treatment were used. Total RNA quality was assessed by gel electrophoresis and RNA quantity was determined using a Thermo Scientific Nanodrop Lite Spectrophotometer (Thermo Fisher Scientific, Wilmington, DE). Samples were sent to IGA Technologies Srl (Udine, IT) for RNA sequencing service. TruSeq Stranded mRNA kit (Illumina, San Diego, CA) was used for library preparation following the manufacturer's instructions. RNA samples were quantified and quality tested by Agilent 2100 Bioanalyzer RNA assay (Agilent Technologies, Santa Clara, CA). Final libraries were checked Agilent Bioanalyzer DNA assay (Agilent Technologies, Santa Clara, CA). Libraries were prepared for sequencing and sequenced on single-end 75 bp mode on NextSeq 500 (Illumina, San Diego, CA). Alignment of reads to the reference transcriptome available on Cucurbitgenomics database (http://cucurbitgenomics.org/)[23] was performed using STAR software with default parameters. The resulting raw data have been normalized and the differentially expressed genes were identified using a 2.3 threshold of FPKM data (in log2). Data have been deposited in the NCBI GEO database (accession number GSE173716).

A student *t* test was applied for analysis of homogeneity of variance, statistical analysis for scatter plots, box and whiskers graphs. A principal component analysis (PCA) was performed with R statistical software (www.r-project.org). Venny bioinformatics tool (http://bioinfogp.cnb.csic.es/tools/venny/) was used for the generation of Venn diagrams. Gene Ontology (GO) analysis and *A. thaliana* ortholog gene identification was performed by the Cucurbitgenomics database. The GO term enrichment analysis was conducted using a cut-off p-value of 0.05 for cellular components and biological processes, and 0.03 for relevant pathways,

respectively. Network analysis was performed using the GeneMANIA data service (http://www.genemania.org/) using *A. thaliana* orthologues genes.

Samples preparation for synchrotron-based analyses

μ-XRF and XANES analyses were performed at ELETTRA, Sincrotrone Trieste, in order to analyse Cu presence and distribution in tissues; root, leaf and flower samples (0.1 g, fresh weight) were cut and submerged in glutaraldehyde triphosphate in Eppendorf tubes for fixation. After three days the samples were dehydrated in gradients of alcohol (from 25 to 100%) and fixed with epoxy resin following Kurth et al. (2009).[24] To analyse potential variations in local structures within the tissues, bulk X-ray Absorption Spectroscopy (XAS) analyses at BM08 "LISA" beamline at ESRF have been performed. The protocols described in Marmiroli et al. (2020)[25] were applied. Briefly, samples were mixed with pure cellulose powder (Sigma Aldrich, St. Louis, MO, USA) and pressed into 1.3 cm diameter pellets using an amount of material sufficient to keep the total absorption (μ) ≤1.5 above the edge.

Low Energy μ-XRF (LE μ-XRF)

μ-XRF analyses in the soft X-ray regime were performed at the TwinMic beamline at ELETTRA, Sincrotrone Trieste, Italy.[26] For the present experiment, the TwinMic microscope was operated in scanning transmission mode (SXM), the beam was focused on the sample through a zone plate (600 μm in diameter with a 50 nm outermost zone width), and a micrometric or sub-micrometric probe size was delivered. While the sample was raster-scanned perpendicularly to the incoming monochromatic beam, a fast readout CCD camera collected the transmitted X-rays and an 8-silicon drift detector-based XRF system acquired the emitted fluorescence photons.[27] The obtained absorption and phase contrast images outline the morphological features of the sample at sub-

229 micrometer length scales, whereas the simultaneous detection of the low energy μ-XRF correlates the
230 elemental distribution to the morphology. The elemental distribution was then obtained by
231 deconvolving and fitting the XRF spectra with PyMCA software.[28] A photon energy of 1.26 keV was
232 used to excite and obtain optimal emission conditions for the elements of major interest (Cu, Na, Ni
233 and Fe) with a spot size of 1.45 μm and a dwell time of 8 s per pixel for XRF mapping and a CCD
234 dwell time of 50 ms per SXM imaging. Each map lasted approximately 5-7 h, depending on the
235 dimensions of the scanned area.

236

237 *XRF and X-ray absorption near edge structure (XANES) mapping*

238 Zucchini root and flower thin section samples were also investigated by means of XRF
239 mapping and XAS at the XRF beamline, ELETTRA Sincrotrone Trieste (Italy)[29] which covers a
240 different energy range compared to TwinMic and allows detection of heavier elements and K lines of
241 transition metals. The experiment was conducted using a Si(111) monochromator and standard
242 45º/45º geometry for fluorescence mode measurements, using an XFlash 5030 SDD (Bruker, Berlin,
243 Germany). Higher order harmonics contamination was suppressed by a pair of parallel plane mirrors
244 intercepting the beam in grazing incidence. Thin sections of samples embedded in resin were sealed
245 between two Mylar foils and fixed on the Al sample holder using a Delrin interlocking ring. This
246 design was necessary to secure the samples and to have a system compatible with the working
247 conditions of the Ultra High Vacuum Chamber (UHVC, 10^{-7} mbar) available at the XRF beamline.
248 XRF maps were collected with an incident beam energy of 10 keV and a beam size at the exit slits of
249 200x100 μm^2 (HxV) to inspect the elemental distribution. Based on the XRF maps acquired on the
250 samples (data not shown), the areas with higher content of Fe, Cu and Zn were selected to collect
251 XANES spectra at the relative K-edges. The Si(111) monochromator was calibrated before the
252 measurements using reference metal foils. All spectra were collected using 5 seconds per step and a
253 variable energy step as a function of the energy: Large step (5 eV) in the first 200 eV of the spectrum,

254 smaller step (0.2 eV) in the near-edge region and a k-constant step of 0.07 $Å^{-1}$ further above the
255 absorption edge. Multiple spectra were collected and merged in order to increase the signal to noise
256 ratio. The oxidation state was determined using least-squares Linear Combination Fitting (LCF) based
257 on reference spectra collected on compounds of known oxidation state. Background removal,
258 normalization of XANES spectra and LCF analyses were performed using the ATHENA software
259 package.[30]

260

261 *Extended X-ray absorption fine structure (EXAFS)*

262 Extended X-ray absorption fine structure (EXAFS) measurements at the Cu K-edge (8978.9
263 eV) were performed at the LISA CRG beamline (BM08)[31] at the European Synchrotron Radiation
264 Facility (ESRF, Grenoble, France) using plant samples and three model compounds: CuO (bulk),
265 CuO NPs and $CuSO_4 \cdot 5H_2O$. The main optical features of the beamline were a fixed exit
266 monochromator with a pair of Si(111) crystals (energy resolution $\Delta E/E \approx 1.33 \cdot 10^{-4}$); Si mirrors were
267 used for harmonics rejection (E cutoff ≈ 15 KeV). Energy was calibrated with a Cu reference foil
268 (8978.9 eV). Spectra of plant samples were acquired at 80 K, in order to minimize beam-induced
269 damage, with a constant k step of 0.05 $Å^{-1}$ up to a maximum k value of 12.5 $Å^{-1}$; model compounds
270 were measured at room temperature with a k step of 0.03 $Å^{-1}$ up to k=18 $Å^{-1}$. Plant samples were
271 measured in fluorescence mode with a 12-element HP-Ge detector,[32] while model compounds were
272 measured in transmission mode. Multiple spectra were collected and merged in order to increase the
273 signal to noise ratio. ATHENA software[30] was used to calibrate the energy and to average multiple
274 spectra. Standard procedures were followed to extract the structural extended EXAFS signals
275 ($k \cdot \chi(k)$), including pre-edge background removal, spline modelling of bare atomic background, edge
276 step normalization, and energy calibration.[33] Model atomic clusters centered on the absorber atom
277 were obtained by ATOMS;[34] theoretical amplitude and phase functions were generated using the

278 FEFF8 code.[35] EXAFS spectra were fitted through the ARTEMIS software in the Fourier-Transform
279 (FT) space.[30]

280

281 **Results and Discussion**

282 *Pollen morphology and viability*

283 Pollen grain morphology was analysed by ESEM of transverse sections of developing mature
284 anthers; no overt differences were observed across treatments (Figure S2a). Pollen viability was also
285 evaluated to determine the male gametophyte developmental stage and the preservation of plant
286 reproductive fitness. Similar to morphology, there were no differences across CuO NP, CuO bulk and
287 $CuSO_4$ treatments as compared to the untreated control, with a pollen viability approximately 100%
288 in all cases (Figure S2b).

289 Previous studies have demonstrated that copper can be toxic to seed and pollen germination,
290 pollen viability and pollen tube growth; Sharafi (2014)[36] showed that high concentrations (250 mg
291 Kg^{-1}) of copper cause an almost complete inhibition of pollen germination and pollen tube
292 lengthening in almond (*Prunus dulcis* (Mill.) D.A. Webb cultivars). Similar results were observed in
293 *Pisum sativum*, where copper (35-700 mg Kg^{-1}) was highly toxic to pollen germination.[37] It is unclear
294 if zucchini exhibits a unique tolerance to copper; importantly, few studies have investigated the
295 potential effects of copper nanomaterials on pollen formation and maturation. Kumbhakar *et al.*
296 (2016)[38] showed that both copper and cadmium-based NPs reduced pollen fertility in black cumin
297 (*Nigella sativa* L.), both during pollen formation and in developmental maturation process. Similarly,
298 in *Coriandrum sativum* L. CdS NPs and CuO NPs induced physiological alterations and cytological
299 aberrations in meiotic cells, and decreased viability of pollen.[39] The alteration types and frequencies
300 in meiotic cells of *C. sativum* following NPs treatments (0.25-1 mg L^{-1}) were less severe than those
301 reported in *Nigella sativa*.[38] Notably, in the present study the Cu concentration used was specifically
302 selected to be below the limit considered for Cu contamination in soil.[19-20]

303

304 *Plant biomass and metal content*

305 After flowering, plants were harvested, and the fresh mass of roots and shoots was measured
306 (Table S1-S2). Treatment with CuO, CuO NPs and $CuSO_4$ had no impact on zucchini biomass (fresh
307 weight) compared to untreated control. These results align with much of the present literature,
308 showing that exposure to CuO NPs did not negatively impact the biological parameters in agricultural
309 crops. Tamez et al. (2019)[40] reported no significant changes in zucchini root and leaf biomass upon
310 exposure to comparable concentrations of CuO NPs. Pagano et al. (2016)[21] demonstrated that CuO
311 NPs had no effect on *C. pepo* biomass at a higher concentration (500 mg Kg^{-1}) and with an
312 experimental design that provided greater direct interaction between NPs and tissues (vermiculite
313 growth media). Alternatively, studies conducted with the model plant *Arabidopsis thaliana* grown in
314 hydroponic conditions showed a strong reduction in root length after exposure to CuO NPs (10-20
315 mg L^{-1}).[41] These contrasting results demonstrate the importance of CuO NPs dose to biological
316 response, and also highlight the influence of growth medium, plant species, and the exposure time to
317 observed effects.

318 The Cu content in soil and in the different tissues of zucchini plants was determined by Atomic
319 Absorption Spectroscopy (AAS), as shown in Table S3. The Cu content in soil was determined (14.18
320 mg Kg^{-1}) in order to justify the concentrations utilized for the experiment, highlighting a different
321 metal release percentage within the soil, starting from the same relative concentration of Cu
322 potentially available of 80 mg Kg^{-1} (salt > NP > bulk). Although there was a trend for increased Cu
323 content of tissues with all Cu treatments, only plant roots from the $CuSO_4$ exposure were significantly
324 increased. To validate the AAS results on flowers, analysis of the Cu content was performed also by
325 Inductively Coupled Plasma Mass Spectrometry (ICP-MS). Here, results show that the Cu content
326 from the CuO NPs and bulk material treatment was 43 and 30% (significant at $p<0.05$) greater than
327 the untreated control, respectively (Table S4). This finding demonstrates that CuO NPs addition to
328 the soil does result in Cu accumulation in the reproductive tissues, although there is no difference

based on particle size. However, these results were impacted by instrument limits of detection (ICP-MS: 0.04 μg L^{-1} vs AAS: 0.05 mg L^{-1}) and quantitation (ICP-MS: 0.1 μg mL^{-1} vs AAS: 0.1 mg L^{-1}). A previous study from our group focused on zucchini exposed to nanoscale Cu evaluated a broad set of physiological assays, including chlorophyll content, mitochondrial functionality, and metal content in different plant tissues (roots, stems, leaves), and also demonstrated significant Cu translocation from roots to both stems and leaves.[21]

RNA-seq data analysis: critical aspects related to the CuO NP molecular response

Given the evidence of an active translocation of Cu into reproductive tissues, the plant transcriptomic response of different tissues and organs to exposure was evaluated using the high-quality assembly of the *C. pepo* genome (NCBI BioProject PRJNA386743, sequences length 263 Mbps; 34240 ORFs) published on Cucurbitgenomics database.[23] Statistical analysis of RNA-seq datasets showed high homogeneity between treatments in the different tissues, with comparable averages and dispersions (Figures S3-S6). After normalization to the untreated control, comparison across CuO NPs, CuO bulk and $CuSO_4$ exposure in roots showed 4420, 6540, and 4747 differentially expressed genes in the three treatments, respectively. In leaves, the CuO NPs treatment showed a lower number of differentially expressed genes compared to the other treatments: 3122 genes were up- or down-regulated with CuO exposure, whereas the values for CuO bulk and $CuSO_4$ were 9924 and 9103, respectively. The number of differentially expressed genes in CuO NPs exposed pollen was also markedly lower in comparison to the treatments in the other tissues: 1829, 2112 and 2163 respectively for CuO NPs, CuO bulk and $CuSO_4$ treatments. This large quantitative difference in gene expression was certainly related with a larger number of different biological processes performed in roots and leaves, as compared to pollen, but could be also due to the lower amount of the Cu (in different forms) translocated to pollen.

Venn diagrams of up- and down-regulated genes in roots (Figure 1) and the relative GO enrichment (Supplementary Information, SI2) data show that the transcripts in common among all the tested conditions were only 4.3% and 16.3% of total genes up- and down-regulated, respectively. In the roots, the specific molecular responses to the three different treatments were largely independent of each other, as shown by the low percentage of gene functions common among all the three conditions tested and by the two-by-two common classes. Metabolic processes and ribosome translation were the most highly represented groups in biological processes related to CuO NPs and CuO bulk (Figure 2; details in Supplementary Information, SI2), together with mitochondrial activity. In the $CuSO_4$ treatment, unlike the NPs and bulk exposure, a nuclear component was represented, and this can be related to greater Cu ion toxicity.[42] The percentage of genes commonly up- or down-regulated in leaves was similar to that observed in roots: 4.7% and 16.4% total shared genes, respectively (Figure 1). The percentage of genes in common between CuO bulk and $CuSO_4$ increased dramatically, both for up- and down-regulated transcripts, to 40.1% and 46.6%, respectively. This observation may correlate with the Cu ion release from the CuO bulk material within the plant tissues, which seems to be higher than for CuO NPs, in spite of the similar dissolution rate in ddH_2O. Genes involved in metabolic and energetic processes are among the more enriched genes; in addition, GO terms related to chloroplast genes are well represented, as are genes for abiotic stimuli response (Figure 2; details in Supplementary Information, SI3). Previous studies with *A. thaliana* highlighted the role of chloroplast as a potential target of ENMs exposure.[43] Wang *et al.* (2016)[44] showed that CuO NPs block electron transport between the two photosystems which can cause an excessive ROS accumulation and oxidative stress, damaging biological molecules and disrupting of cellular metabolism. Furthermore, CuO NPs strongly up-regulate ZAT12, a transcription factor implicated in abiotic stress response, with a key role in ROS signalling pathway and co-expressed with ORF31, a chloroplastic electron carrier involved in photosynthesis that has been identified as a potential biomarker of ENM exposure.[21] In pollen, the percentage of genes up- or down-regulated common to all treatments increased as compared to the leaves and roots: 25.5% and 33%, respectively (Figure

1). The percentage of genes up- and down-regulated specifically related to CuO NPs response is significant (21.1% and 12.5%), when compared to the other two treatments. This data strengthens the idea that CuO NPs were not only translocated (intact or modified) into the floral parts of the plant, but once there, they trigger a "nanoscale-specific" response which is different from the response observed in roots and leaves. These results likely reflect a multifaceted response, including partial dissolution of CuO NPs and CuO bulk giving rise to a "non-specific Cu response", along with a non-dissolved component exerting a nanoscale-specific response. It is also reasonable to suppose that amount of Cu^{2+} derived from the three treatments increased as a consequence of the interaction with plant organs and tissues.

Pollen has a significantly lower number of expressed genes as compared to the vegetative tissues, but data highlight some pollen-specific functions and other components which have been described as unique to sporophyte tissues.[45] The difference between the leaves was related to the low level of expression of genes involved in energy metabolism, especially photosynthesis, since pollen is not photosynthetically active. Another difference between treated and untreated plants was in pollen with higher expression level of genes with functions in ion transport, cell-wall and starch metabolism, and cytoskeleton dynamics (Figure 2; details in Supplementary Information, SI4). Previous studies showed that polarized internal gradients and/or external fluxes of protons, potassium, and chloride had a role in pollen tube function,[46] but that ion channel and transporter involvement in ion fluxes across the plasma membrane in pollen tubes is still largely unknown. Starch biosynthesis during the final phases of pollen maturation is fundamental because starch is a reserve source of energy for pollen survival and it may also act as a metabolic checkpoint for pollen maturity. This pathway is prematurely aborted whenever starch levels remain below a critical amount, strongly linking pollen viability to starch deficiency.[47] A key aspect of pollen tube tip growth is the constant construction of new cell wall and plasma membrane at the tube apex. Vesicles delivering this material are mediated by the actin cytoskeleton.[48]

The whole transcriptome analysis of *C. pepo* treated with CuO NPs showed interesting insights from a functional point of view. Chloroplast and mitochondrial function were critical in regulating the response to CuO NPs and the energy metabolism in all plant tissues, which becomes primarily mitochondrial functionality in pollen formation and development (Figure 2; details in Supplementary Information, SI5). A network analysis produced for chloroplast genes in leaves, and for mitochondrial genes in roots, leaves and pollen, respectively, shows the physical interactions between the reported gene targets (Figures S7-S10). Genes highlighted in heatmaps and Venn diagrams (Figure 3) showed a certain specificity to CuO NPs response, in particular in roots and leaves. In the case of pollen, the percentage of common regulated genes among CuO NPs, CuO bulk and $CuSO_4$ treatment is increased (Figure 3), suggesting that during translocation from roots to shoots there was an increase in ionic Cu presence. Additional information about potential sensitive targets in pollen development, derived from the study of orthologue genes in the yeast *S. cerevisiae*, were investigated, highlighting a certain level of commonality in the response with the RNA-seq analyses. Results are reported and described in Supplementary information (Table S5, and Figure S11).

CuO NPs biotransformation

μ-XRF analyses performed at the TwinMic beamline,[26] an example of which is depicted in Figure 4, showed that in the root sections, Cu in general was mainly detectable on cell walls and more visible in the treatments with $CuSO_4$, followed by nanoparticle and bulk forms where Cu content was very close to TwinMic detection limits; the higher presence of Cu in the treatments with $CuSO_4$ salt is due to the salt dissociation in the soil and followed by ready Cu accumulation in the roots. Notably, the roots were thoroughly washed before the resin embedding procedures to avoid external contamination. Fe was highly present in all root samples, including the controls, likely because it was abundant in the soil. The roots maps for Cu (Figure 4a) are consistent with those obtained by Servin *et al.* (2017).[18] In the flower samples (Figure 4b), it is possible to observe the pollen sacs and the

429 completely developed pollen grain; one exception is for the $CuSO_4$ treatment, where the pollen sacs
430 were noticeably smaller and possessed fewer pollen grains. Interestingly, Cu was present in the roots,
431 in particular in the cell wall, where other elements such as Ca, which is an important cofactor in
432 building of the cell wall, are known to be present.[49] In CuO bulk treatment Cu was almost not
433 detectable in roots. Although the resolution of the maps does not allow nanoparticle visualization, the
434 EXAFS analyses (Table S6, Figure 5) confirm that CuO NPs in the plants were biotransformed. This
435 suggests that cellular and molecular activities remodel and biotransform the nanoparticles. Cu was
436 present in the flowers treated with all the three types of Cu-based materials, but there were minimal
437 differences in the signal intensity and in the localization of the element. The treatment with CuO NPs
438 did not hinder formation of the flower or pollen and did not result in overt phytotoxicity, but there
439 were nanoscale-specific molecular effects at the transcriptomic levels as described by RNA-seq
440 analysis. The same was true for the bulk Cu treatment, although treatment with $CuSO_4$ did appear to
441 negatively affect gamete formation. The idea of a biotransformation of CuO NPs once within the
442 plant tissues has been reported in the literature; Servin et al. (2017) reported that after treatment,
443 transformed CuO NPs products were detected in roots as Cu_2O, Cu_2S and Cu-acetate.[18] These
444 biotransformation processes significantly influence NPs bioavailability and effects in plants,
445 including broad main metabolic and physiological processes, as well as gametogenesis.[18,50]

446 Figure 5 shows normalized XANES and EXAFS spectra of the plant samples, together with
447 those of the model compounds CuO, CuO NPs and $CuSO_4 \cdot 5H_2O$ and the EXAFS multiparameter fits.
448 Both XANES (results shown in Figure S12) and EXAFS features show that the CuO NPs structure is
449 closely related to the CuO bulk structure. EXAFS multiparameter fits (Table S6) were performed on
450 both CuO samples based on the tenorite structure,[51] yielding the same results in terms of interatomic
451 distances and path degeneracies, with both refined parameters closely agreeing with the theoretical
452 ones. EXAFS quantitative results on plant samples (Figure 5, Table S6) clearly indicate that the CuO
453 structure is not fully preserved within the plants tissues, in particular in the roots, and that after uptake,
454 the particles are biotransformed over time, leading to Cu^{2+} release starting in roots and increasing up

455 to the flower. Specifically, the prominent signal at R > 4.5 Å in the Fourier Transform (FT) spectra
456 in both CuO bulk and NPs is not visible any longer in plant samples. Moreover, the peaks at R< 4.5
457 Å are markedly weakened. In addition, no overt differences are observable among plant samples
458 treated with two different CuO types. First, shell distances in both roots and flowers are typical of
459 Cu^{2+} in square planar coordination with O and thus compatible with a remnant structure of CuO.
460 However, the Cu local environment in the higher shells shows small differences between roots and
461 flowers. Indeed, a second Cu-O shell path is systematically present in both flowers and roots at
462 significantly different distances: ≈2.7 Å in roots and 2.8 Å in flowers. Moreover, a Cu-Cu path at
463 ≈3.55 Å is always present in roots while the same path could not be fitted in flowers, the only
464 exception being plants treated with $CuSO_4$, where the path distance is much longer (3.79 Å). In shoots
465 of the Cu hyperaccumulator plant *Crassula helmsii*, Kupper at al. (2009)[52] reported Cu^{2+} O ligands
466 at 2.001 Å, indicating Cu bonds with small organic acids. Mijovilovich et al. (2009)[53] studied the
467 leaves of *Noccea caerulescences* (ecotype Ganges), an hyperaccumulator plant of Cd and Zn but
468 sensitive to Cu, reported ligands for Cu^{2+} at 1.9 Å sulfur atoms, indicating ligands with S rich
469 molecules, and at 4.5 Å, a double ligand Cu-Cu that they attributed to Cu biomineralization. These
470 findings do not align with our results and this is likely due to plant species differences;
471 hyperaccumulator plants having a unique and specific metabolic profile that is different from that of
472 non-hyperaccumulator species such as *Cucurbita pepo*.

473

474 *Environmental implications*

475 Given the essential role of Cu to the plant life cycle and its biotic response to disease, there
476 has been significant interest in its use as a potential nanofertilizer. However, in certain plants and
477 under certain concentrations, phytotoxicity has been observed. In the present study, the effect of three
478 types of Cu (CuO NPs, CuO bulk, and $CuSO_4$) was compared in *C. pepo* using a broad range of
479 physiological and molecular endpoints, with a focus on the process of male gametogenesis and pollen

480 production, which are essential to reproduction and from fruit formation and ultimately, to plant yield.
481 In a dioic species such as zucchini, gamete fertilization depends primarily on pollen quality and
482 vitality of the parental plant, which then mediates fruit production. From the morphological and
483 physiological perspective, as inferred by ESEM and XRF analyses, there were few differences
484 between the three forms of Cu (CuO NPs, CuO bulk and $CuSO_4$) in the roots, but as the Cu was
485 translocated to the flower, the $CuSO_4$ treatment exerted a more marked negative effect on pollen
486 viability. This increasing toxic response likely was a function of the complete dissolution to Cu^{2+} ions
487 in this medium and the increased reactivity of Cu in this form. Conversely, the NP form exerted
488 almost no effects on pollen and exhibited a reduced stimulation of Cu uptake, possibly being a
489 function of Cu complexed to organic ligands within the plant tissues that mitigated chemical
490 dissolution. The CuO bulk material results for the molecular and physiological endpoints were more
491 similar to $CuSO_4$, in spite of the CuO bulk and CuO NPs dissolution behavior in ddH_2O being quite
492 similar. Interesting, some nanoscale materials release ions at a greater rate than bulk materials, due
493 to increased surface area and volume.[14] However, coatings, complexation and corona formation could
494 modulate dissolution. The transcriptomic analysis of the different tissues and flowers showed that
495 metabolic processes and ribosome translation were highly represented among the most responsive
496 pathways. Chloroplast and especially mitochondrial functions were particularly affected in response
497 to CuO NPs, which agrees with previous data and aligns with the organelle's role in energy
498 metabolism in all plant tissues,[44] and specifically in pollen formation and development. In addition,
499 the EXAFS features demonstrate the occurrence of CuO NPs biotransformation, highlighting a
500 similar Cu local environment from roots to flowers. The similarity of the Cu environment after
501 different treatments seemed to depend more on the plant tissue than on the type of treatment,
502 suggesting that the biotransformed Cu environment is reached after substantial dissolution of Cu ions,
503 followed by stabilization of Cu in complexes whose nature is more dependent on the plant
504 characteristics than on the type of treatment. Indeed, the transcriptomic data showed that at the
505 molecular level, the response was partially nanoscale-specific, including in the pollen. Similar

phenomena have been reported for other nanomaterials such as CeO_2 NPs and CdS QDs.[25,54] The evidence for the formation of Cu ions when CuO NPs are accumulated by the plants and the fact that still there is a certain level of nanoscale-specific response suggests that *in planta* biotransformation processes are significant and critical to overall plant response. Overall, this suggests nanoscale CuO NPs as nanofertilizers likely presents minimal concerns to general plant health. A thorough and mechanistic understanding of these processes such as that provided by this study will be necessary to ensure the safe and sustainable application of Cu-based and other nanoscale materials in nano-enabled agricultural strategies.

Acknowledgements

LP acknowledges the support of FIL ("Fondi Locali per la Ricerca") 2018. MM acknowledges ELETTRA Sincrotrone Trieste beamlines TwinMic (proposal 20195157) and XRF (proposal 20195260) for CuO experiments on zucchini plants. GOL and MM acknowledge for XAS experiments on bulk samples were performed on LISA CRG beamline at the European Synchrotron Radiation Facility (ESRF), Grenoble, France during experiment EV-366. JCW acknowledges USDA Hatch CONH00147. The present study has benefited from the equipment and framework of the COMP-HUB Initiative, funded by the 'Departments of Excellence' program of the Italian Ministry for Education, University and Research (MIUR, 2018-2022).

Authors contribution

MM, LP, NM and JCW coordinated the study and designed the experiments. RR, LP and RD performed individual experiments and analysed the physiological and molecular data in with collaboration of MM and RRu. AG, GA, performed the synchrotron analyses in Trieste with collaboration of SP, GG and VB. AP, FA and GOL (remotely) performed the XAS measurements at

LISA BM08 beamline at ESRF; GOL performed EXAFS data analysis in collaboration with FA. All authors contributed to manuscript revision and approved the final version.

Conflict of interest

The authors declare no conflict of interest.

Supplementary Information (SI) description:

Supplementary information included (SI1):

Method section and results for qPCR of genes involved in gametogenesis

Results of LCF analysis of XANES spectra

Figure S1: CuO nanoparticles visualization by TEM

Figure S2: ESEM micrographs pollen grains and pollen viability assay

Figure S3: Statistics of the genes datasets from roots samples

Figure S4: Statistics of the genes datasets from leaves samples

Figure S5: Statistics of the genes datasets from pollen samples

Figure S6: PCA of all data profiles

Figure S7: Gene network of chloroplast targets observed in leaves treated with CuO NPs

Figure S8: Gene network of mitochondrial targets observed in roots treated with CuO NPs

Figure S9: Gene network of mitochondrial targets observed in leaves treated with CuO NPs

Figure S10: Gene network of mitochondrial targets observed in pollen treated with CuO NPs

Figure S11: Heatmap transciprotmics genes involved in meiosis and gametogenesis

Figure S12: XANES fits and relative K-edge data

Table S1: Biomass of roots and shoots

Table S2: Flower biomass

Table S3: Copper concentration measured in soil, roots, shoots and flowers by AAS

Table S4: Copper concentration measured in flowers by ICP-MS

Table S5: Genes' information and primer sequences utilized in Real time PCR assay

Table S6: EXAFS multiparameter fit details for studied samples and reference compounds

Supplementary information reported in excel format:

Supplementary Information 2 (SI2): GO analysis of up- and down-regulated genes exposed to CuO NPs, CuO bulk and $CuSO_4$ in roots.

Supplementary Information 3 (SI3): GO analysis of up- and down-regulated genes exposed to CuO NPs, CuO bulk and $CuSO_4$ in leaves.

Supplementary Information 4 (SI4): GO analysis of up- and down-regulated genes exposed to CuO NPs, CuO bulk and $CuSO_4$ in pollen.

Supplementary Information 5 (SI5): *A. thaliana* ortholog genes analysis of relevant chloroplast and mitochondrial targets isolated from *C. pepo* exposed to CuO NPs, CuO bulk and $CuSO_4$ in roots, leaves and pollen.

References

1. Lowry, G. V., Avellan, A., Gilbertson, L. M. Opportunities and challenges for nanotechnology in the agri-tech revolution. *Nat. Nanotechnol*., **2019**, 14, 17–522.
2. Adisa, I.; Pullagurala, V.L.R.; Peralta-Videa, J.R.; Dimkpa, C.O.; Ma, C.; Elmer, W.H.; Gardea-Torresdey J.L.; White, J.C. **2019**. Recent advances in nano-enabled fertilizers and pesticides: A critical review of mechanisms of action. *Environ. Sci.: Nano*. 6, 2002.
3. Dimkpa, C.O., Bindraban, P.S. Nanofertilizers: New Products for the Industry? *J Agric Food Chem*. **2018**, 66(26), 6462-6473. doi: 10.1021/acs.jafc.7b02150.

4. Rui, M.; Ma, C.; White, J.C.; Tang, X.; Yang, J.; Jiang, F.; Hao, Y.; Ali, A.; Rui, Y.; Cao, W.; Xing, B. Metal oxide nanoparticles alter peanut (Arachis hypogaea L.) physiological response and reduce nutritional quality: A life cycle study. *Environ. Sci.: Nano*. **2018**, 5, 2088-2102.
5. Keller, A.A.; McFerran, S.; Lazareva, A.; Suh, S. Global life cycle releases of engineered nanomaterials. *J. Nanopart. Res.*, **2013**, 15, 1692−1709.
6. Gardea-Torresdey, J.L.; Rico, C.M.; White, J.C. Trophic transfer, transformation, and impact of engineered nanomaterials in terrestrial environments. *Environ. Sci. Technol*., **2014**, 48, 2526–2540.
7. Hawthorne, J.; De la Torre Roche, R.; Xing, B.; Newman, L.A.; Ma, X.; Majumdar, S.; Gardea-Torresdey, J.; White, J.C. Particle-size dependent accumulation and trophic transfer of cerium oxide through a terrestrial food chain. *Environ. Sci. Technol*. **2014**, 48, 13102-13109.
8. Ma, C.; White, J.C.; Zhao, J.; Zhao, Q.; Xing, B. Uptake of Engineered Nanoparticles by Food Crops: Characterization, Mechanisms, and Implications. *Annu. Rev. Food Sci. Technol*. **2018**, 9, 129–53.
9. Majumdar, S.; Ma, C.; Villani, M.; Zuverza-Mena, N.; Pagano, L.; Huang, Y.; Zappettini, A.; Keller, A.A.; Marmiroli, N.; Dhankher, O.P.; White, J.C. Surface coating determines the response of soybean plants to cadmium sulfide quantum dots. *NanoImpact*, **2019**, 14, 100151. Doi: 10.1016/j.impact.2019.100151.
10. Servin, A. D.; White, J. C. Nanotechnology in agriculture: Next steps for understanding engineered nanoparticle exposure and risk. *NanoImpact*. **2016**, 1, 9−12.
11. Elmer, W.; De la Torre-Roche, R.; Pagano, L.; Majumdar, S.; Zuverza-Mena, N.; Dimkpa, C.; Gardea-Torresdey, J.; White, J. C. Effect of metalloid and metallic oxide nanoparticles on Fusarium wilt of watermelon. *Plant Dis.* **2018**, 102 (7), 1394−1401.
12. Kah, M.; Tufenkji, N.; White, J.C. Nano-enabled strategies to enhance crop nutrition and protection. *Nat. Nanotechnol*., **2019**, 14, 532–540.

13. Ma, C.; Borgatta, J.; Hudson, B.G.; Abbaspour-Tamijani, A.; De La Torre-Roche, R; Zuverza-Mena N.; Shen, Y.; Elmer, W.; Xing, B.; Mason, S.E.; Hamers, R.J. White J.C. Advanced material modulation of nutritional and phytohormone status alleviates damage from soybean sudden death syndrome. *Nat. Nanotechnol*. **2020**. Doi: 10.1038/s41565-020-00776-1.

14. Borgatta, J.; Ma, C.; Hudson-Smith, N.; Elmer, W.; Plaza Perez, C.D.; De La Torre-Roche, R.; Zuverza-Mena, N.; Haynes, C.L.; White, J.C.; Hamers, R.J. Copper Based Nanomaterials Suppress Root Fungal Disease in Watermelon (Citrullus lanatus): Role of Particle Morphology, Composition and Dissolution Behavior. *ACS Sus Chem Eng* **2018,** 6 (11), 14847-14856. Doi: 10.1021/acssuschemeng.8b03379

15. Ma, C.; Borgatta, J.; De La Torre-Roche, R.; Zuverza-Mena, N.; White, J.C.; Hamers, R.J; Elmer, W. Time-Dependent Transcriptional Response of Tomato (Solanum lycopersicum L.) to Cu Nanoparticle Exposure upon Infection with Fusarium oxysporum f. sp. Lycopersici. *ACS Sus Chem Eng* **2019,** 7 (11), 10064-10074. Doi: 10.1021/acssuschemeng.9b01433.

16. Huang Y.; Zhao, L.; Keller, A.A. Interactions, Transformations, and Bioavailability of Nano-Copper Exposed to Root Exudates. *Environ Sci Technol*., **2017** 51 (17), 9774-9783. Doi: 10.1021/acs.est.7b02523.

17. Huang, Y.; Li, W.; Minakova, A.S.; Anumol, T.; Keller, A.A. Quantitative analysis of changes in amino acids levels for cucumber (*Cucumis sativus*) exposed to nano copper. *NanoImpact*, **2018**, 12, 9-17. doi: 10.1016/j.impact.2018.08.008.

18. Servin, A.D.; Pagano, L.; Castillo-Michel, H.; De la Torre-Roche, R.; Hawthorne, J.; Hernandez-Viezcas, J.A.; Loredo-Portales, R.; Majumdar, S.; Gardea-Torresdey, J.L.; Dhankher, O.P.; White, J.C. Weathering in soil increases nanoparticle CuO bioaccumulation within a terrestrial food chain. *Nanotoxicology*, **2017**, 11, 98–111. Doi: 10.1080/17435390.2016.1277274.

19. McLean, E.J.; Bledsoe, B.E. Behavior of Metals in Soils. *United States Environmental Protection Agency*, **1992**, EPA/540/S-92/018.

20. Shabbir, Z.; Sardar, A.; Shabbir, A.; Abbas, G.; Shamshad, S.; Khalid, S.; Natasha; Murtaza, G.; Dumat, C.; Shahid, M. Copper uptake, essentiality, toxicity, detoxification and risk assessment in soil-plant environment. *Chemosphere*, **2020**, 259, 127436.

21. Pagano, L.; Servin, A. D.; De La Torre-Roche, R.; Mukherjee, A.; Majumdar, S.; Hawthorne, J.; Marmiroli, M.; Maestri, E.; Marra, R. E.; Isch, S. M.; Dhankher, O. P.; White, J. C.; Marmiroli, N. Molecular Response of Crop Plants to Engineered Nanomaterials. *Environ. Sci. Technol.* **2016**, *50* (13), 7198–7207. Doi: 10.1021/acs.est.6b01816.

22. Peterson, R.; Slovin, J. P.; Chen, C. A Simplified Method for Differential Staining of Aborted and Non-Aborted Pollen Grains. *Int. J. Plant Biol.* **2010**, 1 (2), 66–69. Doi: 10.4081/pb.2010.e13.

23. Montero-Pau, J.; Blanca, J.; Bombarely, A.; Ziarsolo, P.; Esteras, C.; Martí-Gómez, C.; Ferriol, M.; Gómez, P.; Jamilena, M.; Mueller, L.; Picó, B.; Cañizares, J. De Novo Assembly of the Zucchini Genome Reveals a Whole-Genome Duplication Associated with the Origin of the Cucurbita Genus. *Plant Biotechnol. J.* **2018**, *16* (6), 1161–1171. Doi: 10.1111/pbi.12860.

24. Kurth, T.; Weiche, S.; Vorkel, D.; Kretschmar, S.; Menge, A. Histology of plastic embedded amphibian embryos and larvae. *Genesis*. **2012**, 50, 235-250. doi:10.1002/dvg.20821.

25. Marmiroli, M.; Lepore, G.O.; Pagano, L.; d'Acapito, F.; Gianoncelli, A.; Villani, M.; Lazzarini, L.; White, J.C.; Marmiroli, N. The fate of CdS Quantum Dots in plants as revealed by Extended X-ray Absorption Fine Structure (EXAFS) analysis. *Environ. Sci.: Nano*, **2020**. Doi: 10.1039/C9EN01433K.

26. Gianoncelli, A., Kourousias, G., Merolle, L., Altissimo, M. & Bianco, A. Current status of the TwinMic beamline at Elettra: a soft X-ray transmission and emission microscopy station. *J. Synchrotron Rad*. **2016**, 23, 1526-1537. doi: 10.1107/S1600577516014405.

27. Gianoncelli, A.; Castaing, J.; Bouquillon, A.; Polvorinos, A.; Walter, P. Quantitative elemental analysis of Della Robbia glazes with a portable XRF spectrometer and its comparison to PIXE methods. *X-Ray Spectrom*., **2006**. 35: 365-369. doi:10.1002/xrs.920.

28. Solé, V.; Papillon, E.; Cotte, M.; Walter, P.; Susini, J. A Multiplatform Code for the Analysis of Energy-Dispersive X-ray Fluorescence Spectra. *Spectrochimica Acta Part B: Atomic Spectroscopy*. **2007**. 62. 63-68. Doi: 10.1016/j.sab.2006.12.002.

29. Karydas, A.; Czyzycki, M.; Leani, J.; Migliori, A.; Osan, J.; Bogovac, M.; Wrobel, P.; Vakula, N.; Padilla A.R.; Menk, R.H.; Gol, M.; Antonelli, M.; Tiwari, M.; Caliri, C.; Vogel-Mikus, K.; Darby, I. An IAEA multi-technique X-ray spectrometry endstation at Elettra Sincrotrone Trieste: benchmarking results and interdisciplinary applications. *J. Synchrotron Radiation*. **2017**. 25. 189. 10.1107/S1600577517016332.

30. Ravel, B.; Newville, M. ATHENA and ARTEMIS: Interactive graphical data analysis using IFEFFIT. *Phys. Scr*. **2006**, 115, 1007-1010. Doi: 10.1238/Physica.Topical.115a01007.

31. d'Acapito, F., Lepore, G.O., Puri, A., Laloni, A., La Mannna, F., Dettona, E., De Luisa, A., Martin, A. The LISA beamline at ESRF. *J. Synchrotron Radiat.* **2019**, 26, 551-558.

32. Puri, A.; Lepore, G. O.; d'Acapito, F. The New Beamline LISA at ESRF: Performances and Perspectives for Earth and Environmental Sciences. *Condens Matter* **2019**, 4, 12-19.

33. Lee, P. A.; Citrin, P. H.; Eisenberger, P. T.; Kincaid, B. M. Extended x-ray absorption fine structure - its strengths and limitations as a structural tool. *Rev Mod Phys* **1981**, 53, 769-806.

34. Ravel, B. ATOMS: crystallography for the X-ray absorption spectroscopist. J Synchr Rad **2001** 8, 314–316.

35. Ankudinov, A.L.; Ravel, B.; Rehr, J.J.; Conradson, S.D. Real-space multiple-scattering calculation and interpretation of x-ray-absorption near-edge structure. *Phys Rev B* **1998**, 58, 7565-7576.

36. Sharafi, Y. Effects of Copper and Leadon Pollen Germination Traits in Almond Cultivars. *J. Nuts Relat. Sci.* **2014**, *5* (2), 67–73.

685 37. Sabrine, H.; Afif, H.; Mohamed, B.; Hamadi, B.; Maria, H. Effects of Cadmium and Copper
686 on Pollen Germination and Fruit Set in Pea (Pisum Sativum L.). *Sci. Hortic.* **2010**, *125* (4),
687 551–555. doi: 10.1016/j.scienta.2010.05.031.
688 38. Kumbhakar, D. V.; Datta, A. K.; Mandal, A.; Das, D.; Gupta, S.; Ghosh, B.; Halder, S.; Dey,
689 S. Effectivity of Copper and Cadmium Sulphide Nanoparticles in Mitotic and Meiotic Cells
690 of Nigella Sativa L. (Black Cumin) – Can Nanoparticles Act as Mutagenic Agents? *J. Exp.*
691 *Nanosci.* **2016**, *11* (11), 823–839. Doi: 10.1080/17458080.2016.1149236.
692 39. Pramanik, A.; Datta, A. K.; Das, D.; Kumbhakar, D. V.; Ghosh, B.; Mandal, A.; Gupta, S.;
693 Saha, A.; Sengupta, S. Assessment of Nanotoxicity (Cadmium Sulphide and Copper Oxide)
694 Using Cytogenetical Parameters in Coriandrum Sativum L. (Apiaceae). *Cytol. Genet.* **2018**,
695 *52* (4), 299–308. Doi: 10.3103/S0095452718040084.
696 40. Tamez C, Hernandez-Molina M, Hernandez-Viezcas J.A, Gardea-Torresday J.L. Uptake,
697 transport, and effects of nano-copper exposure in zucchini (Cucurbita pepo). *Sci Total*
698 *Environ*. **2019**, 665, 100-106. Doi: 10.1016/j.scitotenv.2019.02.029
699 41. Tang, Y.; He, R.; Zhao, J.; Nie, G.; Xu, L.; Xing, B. Oxidative Stress-Induced Toxicity of
700 CuO Nanoparticles and Related Toxicogenomic Responses in Arabidopsis Thaliana. *Environ.*
701 *Pollut.* **2016**, *212*, 605–614. Doi: 10.1016/j.envpol.2016.03.019.
702 42. Dutta, S.; Mitra, M.; Agarwal, P.; Mahapatra, K.; De, S.; Sett, U.; Roy, S. Oxidative and
703 Genotoxic Damages in Plants in Response to Heavy Metal Stress and Maintenance of Genome
704 Stability. *Plant Signal. Behav.* **2018**, *13* (8), 1–17. Doi: 10.1080/15592324.2018.1460048.
705 43. Ruotolo, R.; Maestri, E.; Pagano, L.; Marmiroli, M.; White, J. C.; Marmiroli, N. Plant
706 Response to Metal-Containing Engineered Nanomaterials: An Omics-Based Perspective.
707 *Environ. Sci. Technol.* **2018**, *52* (5), 2451–2467. Doi: 10.1021/acs.est.7b04121.
708 44. Wang, Z.; Xu, L.; Zhao, J.; Wang, X.; White, J. C.; Xing, B. CuO Nanoparticle Interaction
709 with Arabidopsis Thaliana: Toxicity, Parent-Progeny Transfer, and Gene Expression.
710 *Environ. Sci. Technol.* **2016**, *50* (11), 6008–6016. Doi: 10.1021/acs.est.6b01017.

711 45. Honys, D.; Twell, D. Comparative Analysis of the Arabidopsis Pollen Transcriptome. *Plant*
712 *Physiol.* **2003**, *132* (June), 640–652. Doi: 10.1104/pp.103.020925.
713 46. Hepler, PK; Vidali, L; Cheung, AY. Polarized cell growth in higher plants. *Annual Rev. Cell.*
714 *Dev. Biol.* ***2001,*** 17: 159–187
715 47. Wen, L. Y.; Chase, C. D. Mitochondrial Gene Expression in Developing Male Gametophytes
716 of Male-Fertile and S Male-Sterile Maize. *Sex. Plant Reprod.* **1999**, *11* (6), 323–330. Doi:
717 10.1007/s004970050159.
718 48. Da Costa-Nunes, J. A.; Grossniklaus, U. Unveiling the Gene-Expression Profile of Pollen.
719 *Genome Biol.* **2003**, *5* (1), 9–11. Doi: 10.1186/gb-2003-5-1-205.
720 49. Hepler P.K. Calcium: A Central Regulator of Plant Growth and Development. *The Plant Cell*.
721 **2005**, 17(8) 2142-2155. Doi: 10.1105/tpc.105.032508.
722 50. Dai, Y.; Zhao, J.; Liu, X.; Yu, X.; Jiang, Z.; Bu, Y.; Xu, Z.; Wang, Z.; Zhu, X.; Xing, B.
723 Transformation and Species Identification of CuO Nanoparticles in Plant Cells (Nicotiana
724 Tabacum). *Environ. Sci. Nano* **2019**, *6* (9), 2724–2735. Doi: 10.1039/c9en00781d.
725 51. Wyckoff, R. W. G. Crystal Structures 1963. 1, 85–237. Second edition. Interscience
726 Publishers, New York.
727 52. Küpper, H.; Götz, B.; Mijovilovich, A.; Küpper, F.C.; Meyer-Klaucke, W. Complexation and
728 Toxicity of Copper in Higher Plants. I. Characterization of Copper Accumulation, Speciation,
729 and Toxicity in *Crassula helmsii* as a New Copper Accumulator. *Plant. Physiol.* **2009**, 151
730 (2) 702-714. Doi: 10.1104/pp.109.139717.
731 53. Mijovilovich, A.; Leitenmaier, B.; Meyer-Klaucke, W.; Kroneck, P.M.H.; Götz, B.; Küpper,
732 H. Complexation and Toxicity of Copper in Higher Plants. II. Different Mechanisms for
733 Copper versus Cadmium Detoxification in the Copper-Sensitive Cadmium/Zinc
734 Hyperaccumulator *Thlaspi caerulescens* (Ganges Ecotype). *Plant. Physiol.* **2009,** 151 (2),
735 715–731. Doi/10.1104/pp.109.144675.

54. Servin, A.D.; De la Torre-Roche, R.; Castillo-Michel, H.; Pagano, L.; Hawthorne, J.; Musante, C.; Pignatello, J.; Uchimiya, M.; White, J.C. Exposure of agricultural crops to nanoparticle CeO_2 in biochar-amended soil. *Plant Physiol. Biochem*., **2017**, 110, 147-157. Doi: 10.1016/j.plaphy.2016.06.003.

Figure captions:

Figure 1. Comparison of high-throughput transcriptional datasets related to the molecular response of *C. pepo* in condition of treatment with CuO NPs, CuO bulk and $CuSO_4$, in the roots (a), leaves (b), pollen (c), represented with Venn diagrams. Up-regulated and down-regulated genes are reported on left and right side, respectively. Percentage of identity between CuO NPs, CuO bulk and $CuSO_4$ is also reported. Data were normalized on the untreated controls, with a 2.3 threshold of raw data (in log2). Data highlighted an increase in the percentage of common genes involved in the response to the three different Cu-based forms from roots to pollen, suggesting an increased bioavailability of free Cu in the plant shoots.

Figure 2. GO biological processes expressed in percentage (%) of gene cluster enriched, related to roots (a), leaves (b), and pollen (c) related to the treatment with 100 mg kg^{-1} of CuO NPs. Up-regulated and down-regulated genes are reported as blue and orange bars, respectively. Additional details related to GO analyses in the different tissues are available in Supplementary Information, SI2-SI4.

Figure 3. Heatmaps and Venn diagrams comparison of the genes involved in chloroplast functions in response to CuO NPs, CuO bulk and $CuSO_4$, in leaves (a), and in mitochondrial functions identified in roots (b), leaves (c) and pollen (d) tissues. Data related to the specific genes are reported in Supplementary Information, SI5. Data confirmed the increase in percentage of common modulated genes from roots to pollen in response to the three different Cu-based forms utilized for the treatments.

Figure 4. μ-XRF maps of (a) roots and (b) flowers from plants treated with CuO NPs. Names of the mapped elements are on top of each figure. The maps are related to the black and white square on top left (Abs) which is the 20x image of the cells in the root tissue and pollen sac tissues treated with CuO NPs. Cu map is always the last in the second row for (a) and (b).

Figure 5. XANES spectra of the measured samples and model compounds (a). Cu K-edge k^2-weighted EXAFS region (b) and Fourier transforms (c) of plant tissues and model compounds. Solid lines are data, red lines are fits. Energy was calibrated with a Cu reference foil (8978.9 eV). In order to minimize beam-induced damage, spectra of samples were acquired at 80 K with a constant k step of 0.05 $Å^{-1}$ up to a maximum k value of 12.5 $Å^{-1}$ for plant tissues while model compounds were measured at room temperature with a k step of 0.03 $Å^{-1}$ up to k=18 $Å^{-1}$. Plant samples were measured in the fluorescence mode with a 12-element HP-Ge detector.

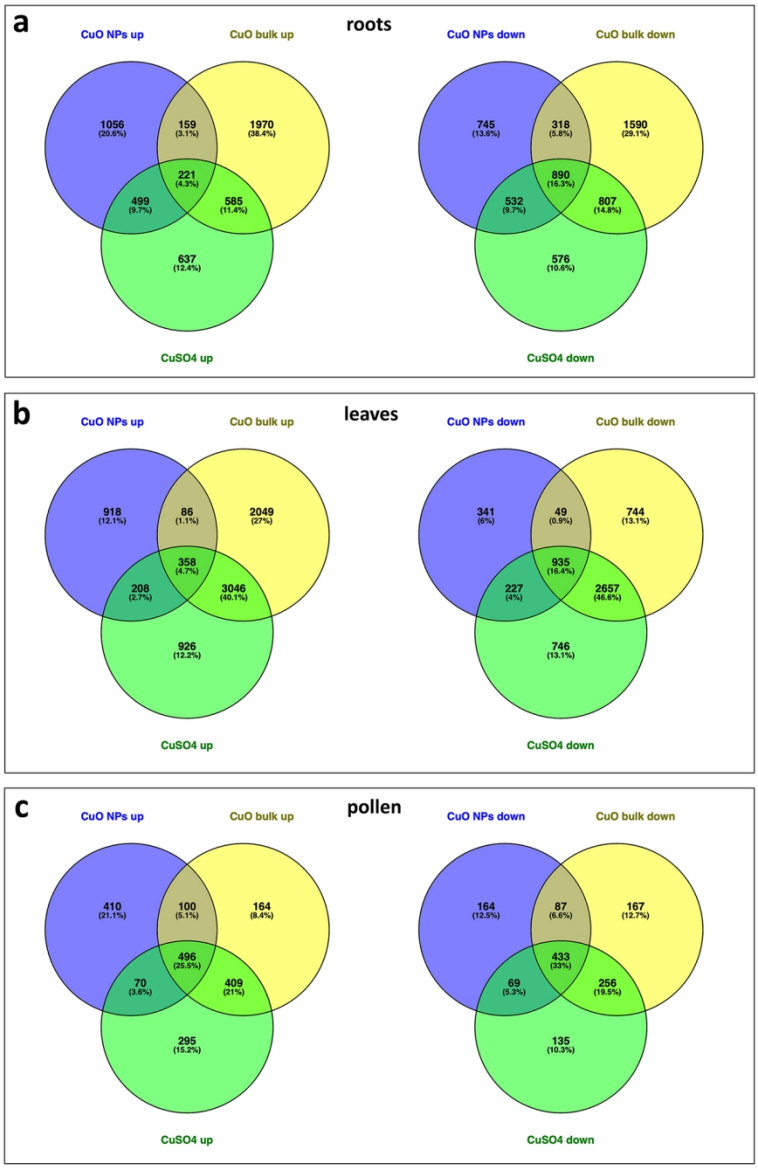

Figure 1. Comparison of high-throughput transcriptional datasets related to the molecular response of C. pepo in condition of treatment with CuO NPs, CuO bulk and CuSO4, in the roots (a), leaves (b), pollen (c), represented with Venn's diagrams. Up-regulated and down-regulated genes are reported on left and right side, respectively. Percentage of identity between CuO NPs, CuO bulk and CuSO4 is also reported. Data were normalized on the untreated controls, with a 2.3 threshold of raw data (in log2). Data highlighted an increase in the percentage of common genes involved in the response to the three different Cu-based forms from roots to pollen, suggesting an increased bioavailability of free Cu in the plant shoots.

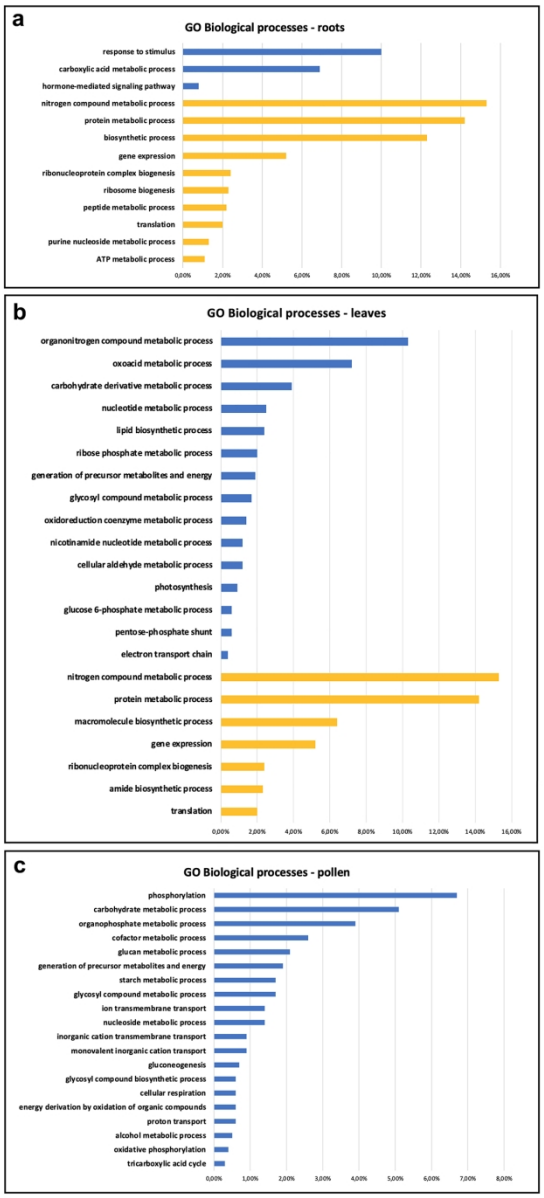

Figure 2. GO biological processes expressed in percentage (%) of gene cluster enriched, related to roots (a), leaves (b), and pollen (c) related to the treatment with 100 mg kg-1 of CuO NPs. Up-regulated and down-regulated genes are reported as blue and orange bars, respectively. Additional details related to GO analyses in the different tissues are available in Supplementary Information, SI2-SI4.

101x223mm (300 x 300 DPI)

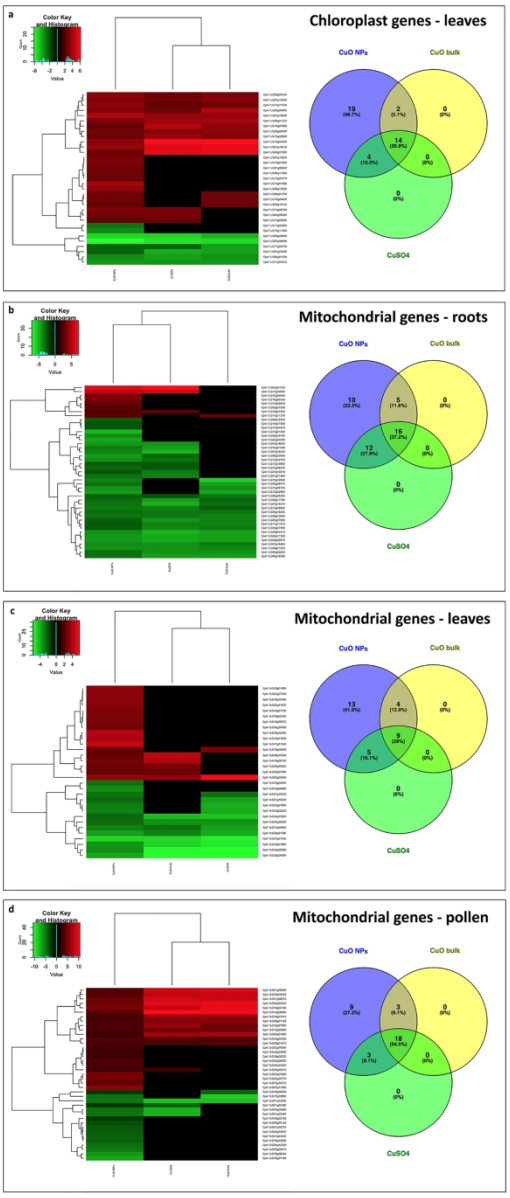

Figure 3. Heatmaps and Venn's diagrams comparison of the genes involved in chloroplast functions in response to CuO NPs, CuO bulk and CuSO4, in leaves (a), and in mitochondrial functions identified in roots (b), leaves (c) and pollen (d) tissues. Data related to the specific genes are reported in Supplementary Information, SI5. Data confirmed the increase in percentage of common modulated genes from roots to pollen in response to the three different Cu-based forms utilized for the treatments.

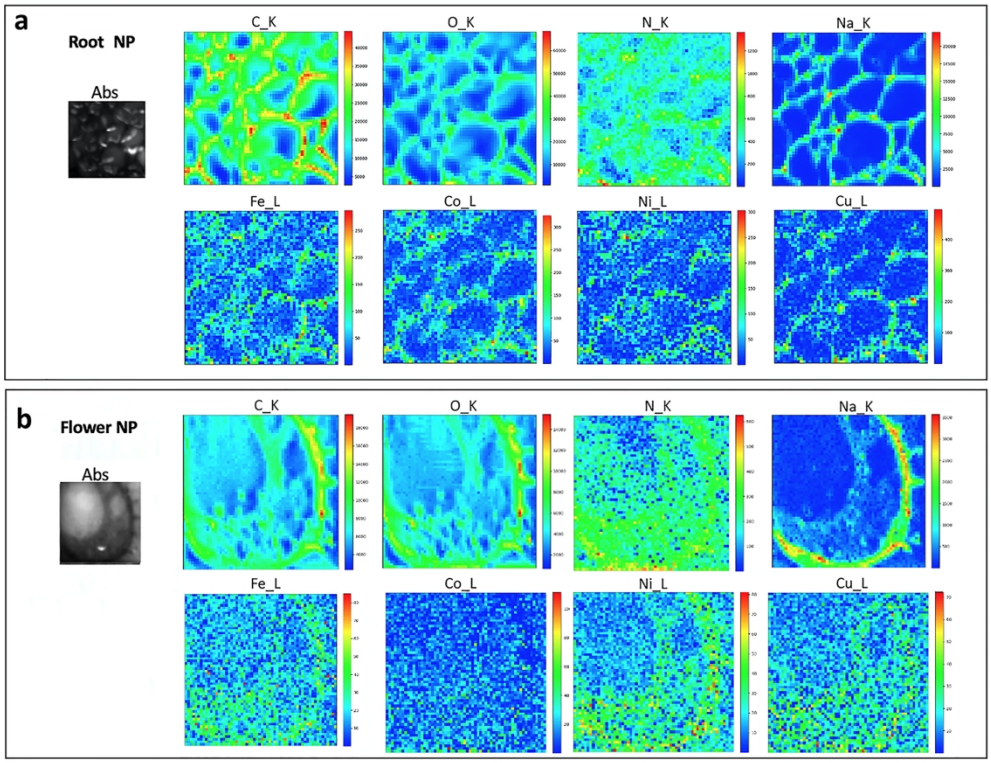

Figure 4. μ-XRF maps of (a) roots and (b) flowers from plants treated with CuO NPs. Names of the mapped elements are on top of each figure. The maps are related to the black and white square on top left (Abs) which is the 20x image of the cells in the root tissue and pollen sac tissues treated with CuO NPs. Cu map is always the last in the second row for (a) and (b).

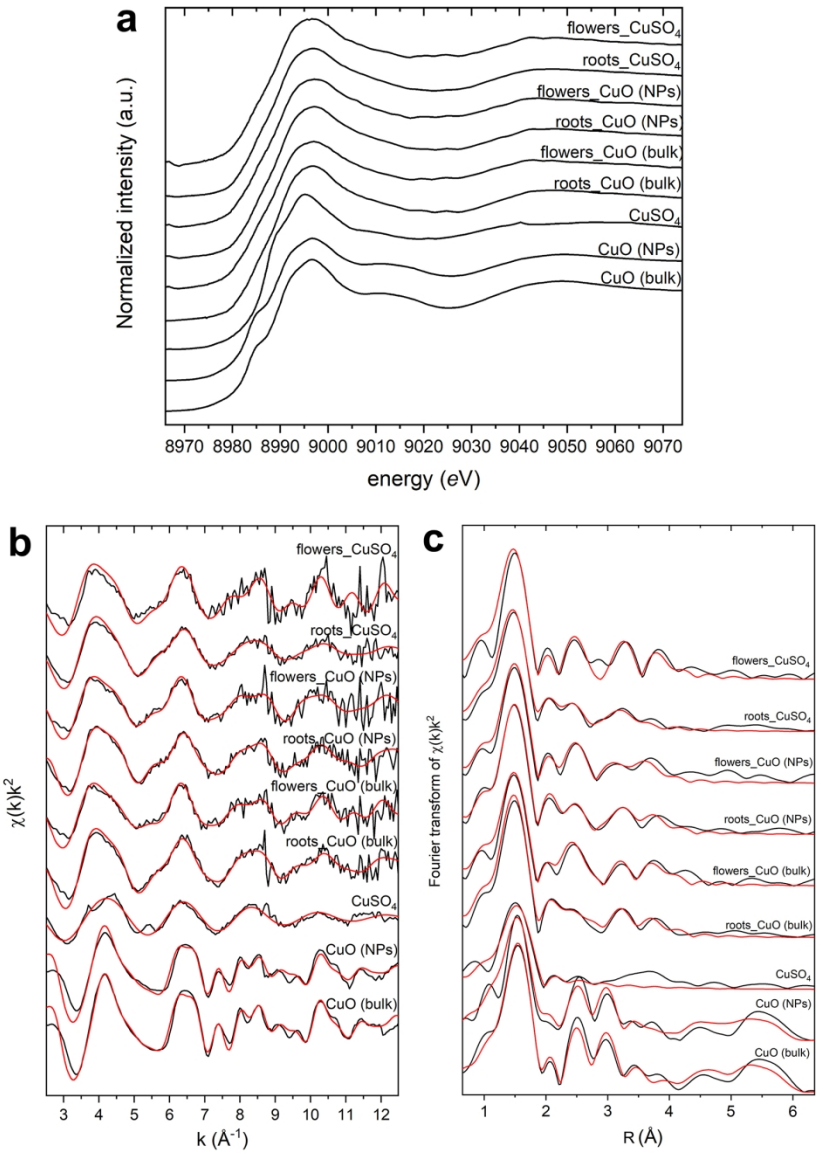

Figure 5. XANES spectra of the measured samples and model compounds (a). Cu K-edge k2-weighted EXAFS region (b) and Fourier transforms (c) of plant tissues and model compounds. Solid lines are data, red lines are fits. Energy was calibrated with a Cu reference foil (8978.9 eV). In order to minimize beam-induced damage, spectra of samples were acquired at 80 K with a constant k step of 0.05 Å-1 up to a maximum k value of 12.5 Å-1 for plant tissues while model compounds were measured at room temperature with a k step of 0.03 Å-1 up to k=18 Å-1. Plant samples were measured in the fluorescence mode with a 12-element HP-Ge detector.